GEOLOGY

Reduced plate motion controlled timing of Early Jurassic Karoo-Ferrar large igneous province volcanism

Micha Ruhl[1,2]*, Stephen P. Hesselbo[3], Hugh C. Jenkyns[2], Weimu Xu[2,4], Ricardo L. Silva[1,5], Kara J. Matthews[2,6], Tamsin A. Mather[2], Conall Mac Niocaill[2], James B. Riding[7]

Past large igneous province (LIP) emplacement is commonly associated with mantle plume upwelling and led to major carbon emissions. One of Earth's largest past environmental perturbations, the Toarcian oceanic anoxic event (T-OAE; ~183 Ma), has been linked to Karoo-Ferrar LIP emplacement. However, the role of mantle plumes in controlling the onset and timing of LIP magmatism is poorly understood. Using global plate reconstruction models and Lower Toarcian sedimentary mercury (Hg) concentrations, we demonstrate (i) that the T-OAE occurred coevally with Karoo-Ferrar emplacement and (ii) that timing and duration of LIP emplacement was governed by reduced Pangean plate motion, associated with a reversal in plate movement direction. This new model mechanistically links Earth's interior and surficial processes, and the mechanism is consistent with the timing of several of the largest LIP volcanic events throughout Earth history and, thus, the timing of many of Earth's past global climate change and mass extinction events.

INTRODUCTION

The Early Toarcian oceanic anoxic event [T-OAE; at ~183 million years ago (Ma)] (*1*, *2*) is recognized as one of the most intense periods of global climatic and environmental disturbance in the past half billion years of Earth's geological history, with geographically widespread oceanic redox change and accompanying large-scale (photosynthetically derived, ^{12}C-enriched) organic carbon burial. Major perturbations to the global carbon cycle at this time have been tentatively linked to volcanism of the Karoo-Ferrar large igneous province (LIP; Fig. 1) and the associated release of isotopically light (^{13}C-depleted) volcanogenic CO_2, thermogenic methane (CH_4) from sill intrusions into Gondwanan coals, and biogenic methane from the dissociation of subseafloor clathrates (*3*–*5*). Temporal variations in the balance of carbon burial and release explains the typical carbon-isotope profile, wherein the Early Toarcian (relatively short-lived) major negative carbon-isotope excursion (CIE) occurs superimposed on a longer-term positive CIE (Fig. 2) (*6*–*8*). The hypothesized tripling of atmospheric pCO_2 (*4*) led to warming of 4° to 10°C in seawater temperatures, even at low- to mid-latitudes (*9*–*11*), and a substantially reduced ocean water pH with a decreased saturation with respect to calcium carbonate ($CaCO_3$) (*12*, *13*). Coeval environmental change on land led to an enhanced hydrological cycle, silicate weathering, vegetation change, and changes in the prevalence of wildfires (*1*, *6*, *14*–*19*). This combined climatic and environmental forcing caused the T-OAE to be accompanied by a second-order mass extinction (*20*, *21*).

The primary cause of the T-OAE is thought to be LIP volcanism in the Karoo-Ferrar region based on overlapping ages assigned to Lower Toarcian marine and continental sedimentary archives (*17*, *22*) and volcanogenic rocks (*5*, *23*). In detail, a temporal and causal relationship is, however, poorly constrained because of limitations in biostratigraphical accuracy and geochronological precision. Furthermore, little is known about the processes that controlled the timing of emplacement of the Karoo-Ferrar LIP, with geochemical evidence suggesting that magmatism arose from mantle plumes beneath the southern African and Antarctic cratons.

Sedimentary archives from both hemispheres, spanning the T-OAE interval, show substantial enrichments in mercury (Hg). Mercury is a volatile element naturally released into the ocean-atmosphere system predominantly from direct volcanic degassing, as well as through thermogenic release from dike- and sill-intruded subsurface organic-rich sediments (*24*–*26*), possibly providing a direct sedimentary signal linking LIP volcanism and past global change events (*25*–*32*).

Here, we study the biostratigraphically well-constrained, complete, and expanded upper Pliensbachian and entire Toarcian succession in the Llanbedr (Mochras Farm) borehole of the Cardigan Bay Basin, Wales, UK (from here on termed Mochras; see Supplementary Materials). We establish the sedimentary enrichment of Hg across the upper Pliensbachian and entire Toarcian, including the T-OAE interval, determine its depositional context, and use the new data to assess the role of Karoo-Ferrar LIP volcanism in causing one of the largest global climatic and environmental perturbations of the Phanerozoic Eon. Last, we combine the geochronologically constrained record of Karoo-Ferrar LIP activity with spatially and temporally resolved plate tectonic models and explore changes in continental plate velocities as the likely control on the onset, timing, and termination of LIP emplacement, thereby mechanistically linking Earth's internal and surficial processes.

RESULTS

Toarcian sedimentary mercury enrichment and Karoo-Ferrar magmatism

Multiple sources and sinks, as well as temporary Hg reservoirs, characterize the present-day natural Hg cycle (see also the Supplementary Materials) (*29*, *33*), with direct emissions from volcanism forming one of the most important natural sources of Hg into modern

[1]Department of Geology, Earth Surface Research Laboratory (ESRL) and SFI Research Centre in Applied Geosciences (iCRAG), Trinity College Dublin, The University of Dublin, College Green, Dublin 2, Ireland. [2]Department of Earth Sciences, University of Oxford, South Parks Road, OX1 3AN, Oxford, UK. [3]Camborne School of Mines and Environment and Sustainability Institute, University of Exeter, Penryn Campus, Treliever Road, Penryn, Cornwall TR10 9FE, UK. [4]School of Earth Sciences and SFI Research Centre in Applied Geosciences (iCRAG), University College Dublin, Belfield, Dublin 4, Ireland. [5]Department of Earth Sciences, Clayton H. Riddell Faculty of Environment, Earth, and Resources, University of Manitoba, 125 Dysart Road, Winnipeg, R3T 2N2, Canada. [6]Arctic Institute of North America, University of Calgary, 2500 University Drive NW, ES-1040, Calgary, AB T2N 1N4, Canada. [7]British Geological Survey, Keyworth, Nottingham NG12 5GG, UK.
*Corresponding author. Email: micha.ruhl@tcd.ie

environments. In the present-day ocean, Hg concentrations vary substantially, depending on the proximity to mid-ocean ridges or river outlets (*34*, *35*). Atmospheric Hg can be distributed globally, especially when injected into the stratosphere as an unoxidized gas or in solid form (see the Supplementary Materials for further details) (*24*, *33*, *36*, *37*).

Deposition of Hg from the atmosphere into the ocean can occur following different pathways, including adsorption onto aerosol particles and subsequent removal from the atmosphere through precipitation or through uptake and intermediate storage in plants and soils and a subsequent shuttling to the oceans (*29*, *33*, *35*, *36*, *38*–*41*). Other natural Hg sources in past environments may have included the melting of permafrost or increased continental weathering (*33*).

When reactive Hg^{2+} reaches the ocean, it commonly forms MeHg (methylmercury), which then accumulates in organic matter (OM) and builds Hg-OM (organo-mercury complexes) (*35*, *42*). This organic sequestration pathway for mercury commonly causes Hg concentration curves in sedimentary archives to evolve in parallel with sedimentary total organic carbon (TOC) (*25*, *27*, *43*). For this reason, sedimentary Hg concentrations are often normalized against TOC and reported as Hg/TOC values [e.g., (*25*)]. Although Hg is commonly bound to OM, it can also be sequestered in other forms including notably by (i) clay minerals, (ii) sulfides [such as pyrite (FeS_2), pyrrhotite ($Fe_{(1-x)}S$, $x = 0$ or 0.2), and mackinawite (FeNiS)] under anoxic/euxinic depositional conditions, or (iii) Fe oxyhydroxides (under oxic depositional conditions) ([(*33*, *44*, *45*) and references therein.

LIP volcanism is suggested to have substantially increased the flux of Hg into the paleoenvironment, and sedimentary Hg contents in sedimentary archives have, therefore, been suggested as a proxy for past LIP activity (*25*–*27*, *29*–*31*, *33*, *46*, *47*). Mercury released from LIP emplacement will include substantial quantities from magmatic degassing, but it may also have been released during the intrusive phase through contact metamorphism with subsurface organic-rich sediments (*25*, *28*, *31*, *47*, *48*). Combined, these processes are suggested to have caused a Hg release of ~150 million tons during emplacement of the Karoo-Ferrar LIP (*33*), in addition to ongoing natural background emissions.

Strata representing the T-OAE have been previously studied for their sedimentary Hg content (*25*, *40*), with some records showing highly elevated Hg levels while other coeval records apparently do not. These studies focused, however, primarily on stratigraphically limited archives, spanning predominantly the negative CIEs associated with the Pliensbachian–Toarcian boundary event and the T-OAE, thereby lacking the ideal level of constraint on background environmental and sedimentary Hg variability during this interval. Furthermore, possible changes in depositional environments and associated changes in the primary process of Hg sequestration in these settings are unconstrained, leading to the question of whether observed elevated sedimentary Hg levels record an increased Hg flux from LIP volcanism or whether they predominantly represent a response to local environmental factors and a change in the efficacy of the shuttling of Hg into the marine sedimentary realm (*40*, *41*, *45*).

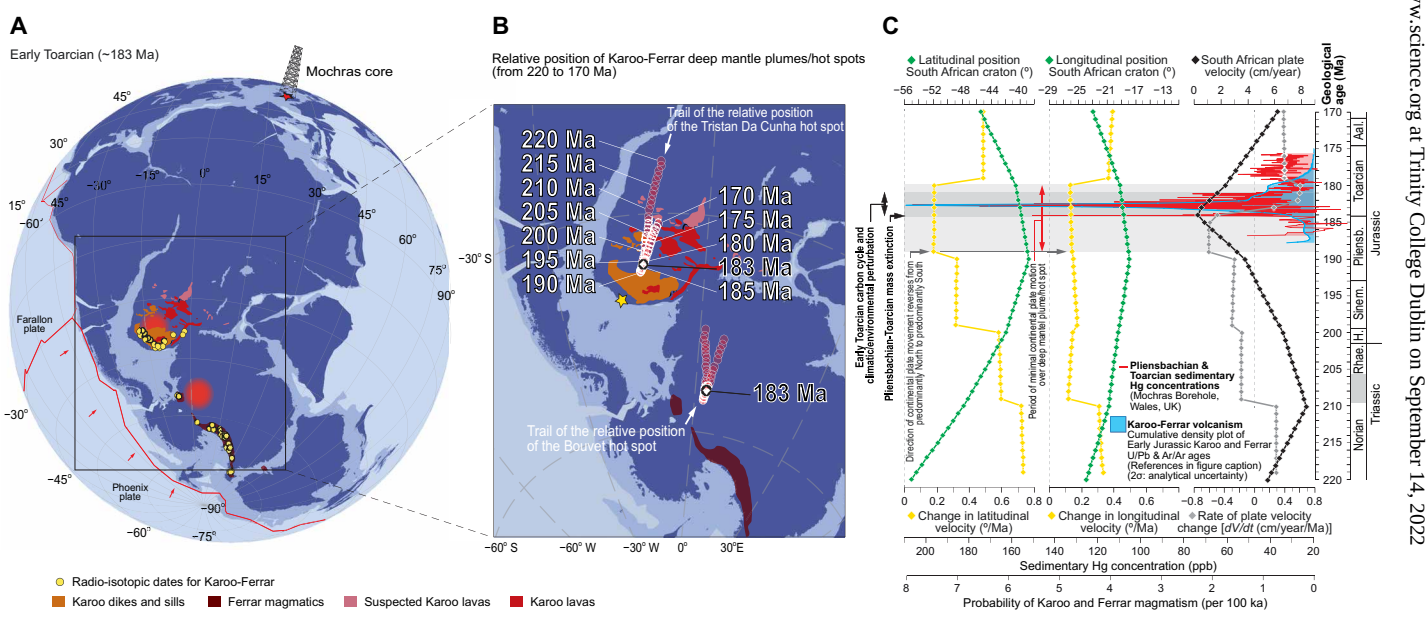

Fig. 1. Late Triassic and Early Jurassic changes in plate motion and the relative position of hot spots. Temporally and spatially resolved plate configuration and velocities based on (*67*, *69*–*72*), imaged here using GPlates, showing a reversal in plate movement direction from predominantly north to predominantly south, in the late Early Jurassic, and an associated reduction in plate velocity. The reduction in local plate velocity, possibly in response to the break-up of Pangea and global plate tectonic processes, was coeval with the emplacement of the Karoo-Ferrar LIP (*5*, *52*–*54*, *56*–*59*). (**A**) Early Jurassic plate configuration. (**B**) Positions of the Tristan Da Cunha and Bouvet hot spots (from 220 to 170 Ma), relative to the overriding plate. (**C**) Evolution of the South African craton latitudinal/longitudinal local plate position, the latitudinal/longitudinal local plate velocity, the absolute local plate velocity, and the rate of local plate velocity change. The absolute reference frame model of (*69*) used here provides rotations for Africa every 10 Ma, which in GPlates are interpolated here for intervening times. Regional paleogeography for the Cardigan Bay Basin (Wales, UK) is given in fig. S1. Yellow star presents locality for which plate movement direction and speed is modeled. Red lines in (A) represent paleo-plate boundaries in the Panthalassic region. (A and B) Present-day coastlines are shaded dark blue for reference; non-oceanic crust is medium blue, and oceanic crust is pale blue. ppb, parts per billion.

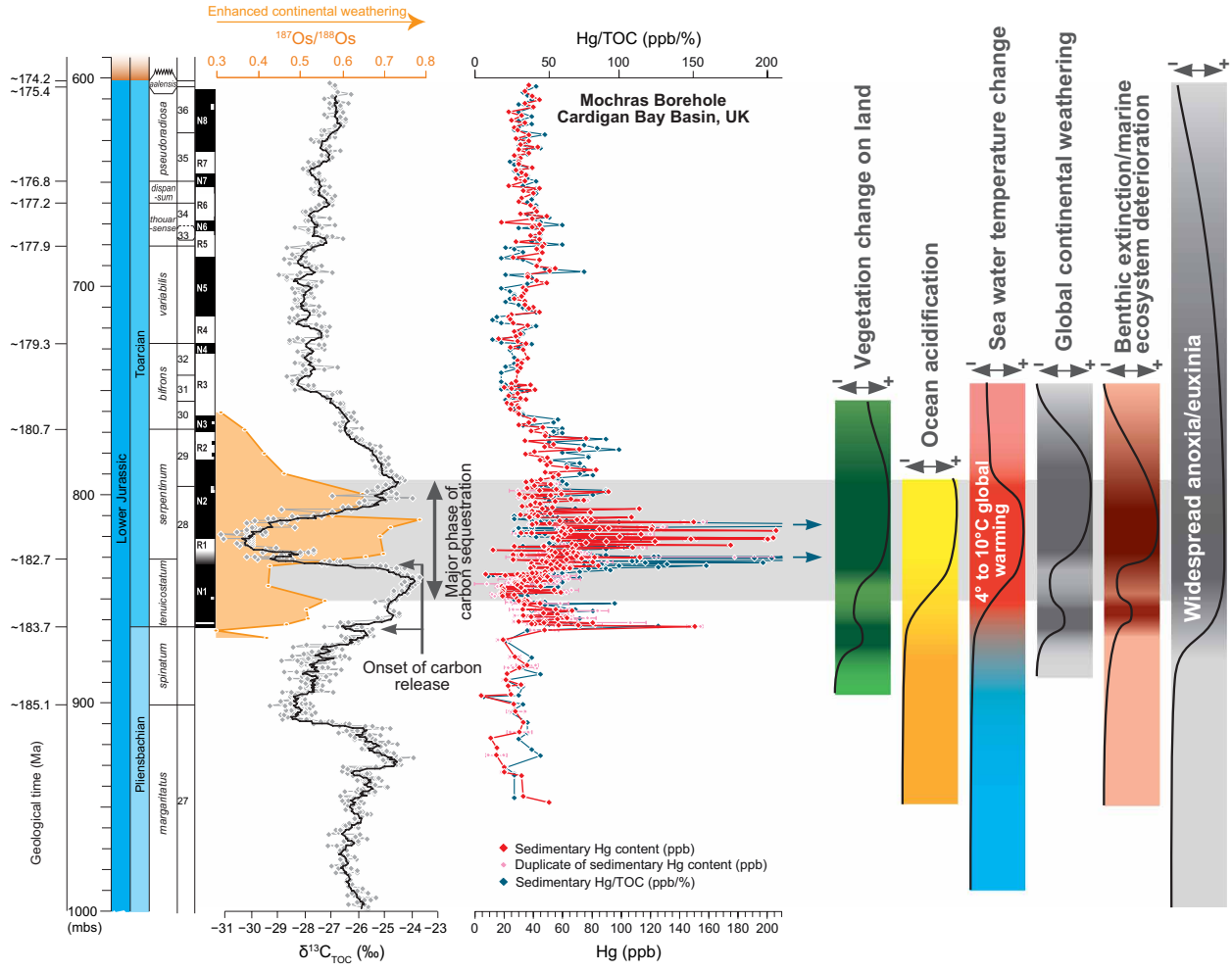

Fig. 2. Changes in Upper Pliensbachian and Toarcian sedimentary Hg concentrations. Sedimentary mercury (Hg) in the Upper Pliensbachian (*margaritatus* zone) and entire Toarcian Stage of the Mochras Borehole, Cardigan Bay Basin, UK (this study), showing overall elevated Hg [and Hg/total organic carbon (TOC)] levels throughout the Lower Jurassic (*tenuicostatum*, *serpentinum*, and lower *bifrons* zones) part of the succession, peaking at the Pliensbachian-Toarcian boundary and during the interval of the negative CIE associated with the Early Toarcian carbon cycle perturbation marking the main phase of the T-OAE. Additional Hg normalizations are provided in fig. S2. Carbon isotope and TOC record are provided in (*7*). Peak Hg/TOC values (blue arrows) are >450 ppb/% and >900 ppb/%, respectively.

Early Toarcian depositional environments were marked by major environmental change due to the widespread development of sub/anoxic and euxinic water columns, rising sea level, and continental weathering rates. Associated changes in detrital sediment supply and strongly increased organic (and inorganic) marine productivity led to elevated carbon sequestration in marine and lacustrine basins. Consequently, Lower Toarcian sedimentary archives are commonly characterized by substantial mineralogical and (bio)geochemical changes.

The biostratigraphically complete and expanded Mochras core of the Lower Jurassic, Cardigan Bay Basin is particularly useful to shed light on whether the Early Jurassic was marked by an elevated Hg loading of the environment as its depositional environment remained relatively unchanged over the studied time interval. In contrast to many other depositional environments at that time, it is characterized by relatively constant marine organic productivity (and preservation) and terrestrial OM supply, only limited changes in (fine-grained) detrital sediment supply (apart from sporadic mass-transport deposits), and no major water column redox changes.

Principal component analyses (PCAs) and nonmetric multidimensional scaling (nMDS) on the combined Mochras core geochemical dataset [including Hg, TOC, hydrogen index (HI), and major and trace element concentrations, e.g., Ca, Si, Fe, Ti, Al, Sr, Rb, S, V, Ni, and Zr] show that sedimentary Hg contents predominantly change in step with the relative abundance of detrital material, i.e., in this case, clay. Changes in the relative abundance of carbonate versus detrital sediment, as reflected in the observed lithological (closed-sum effect) variation, explains >48% [principal component 1 (PC1)] of the total variability in the entire dataset and subdatasets (Fig. 3). The Early Toarcian interval at Mochras [and particularly the upper *tenuicostatum*–lower *serpentinum* (*falciferum*) zone interval] was marked by a reduction in the carbonate flux to the seabed (*7*, *49*), suggesting that a reduction in carbonate dilution is therefore the overall primary control on absolute sedimentary Hg concentrations here, possibly partly explaining the overall increase in values from the (Upper Pliensbachian) top *spinatum* to (Lower Toarcian) lower *bifrons* zones (Fig. 2). The subsequent 12.5% (PC2) of explained variance in the combined dataset

is characterized by a strong concurrent negative loading for TOC and HI. PC3 explains 10.4% of the variance, suggesting an association between the negatively loaded S and Hg and the strongly positively loaded Si, hinting that sulfides and detrital minerals (i.e., clays) are also hosts for sedimentary Hg.

Analysis of specific stratigraphic intervals shows that an 8.6% of the variance (PC3) is explained by a positive loading of Hg versus a negative loading of HI and TOC in the section below the T-OAE negative CIE interval. By contrast, the association of Hg with S, TOC, and Ni in the section above the T-OAE negative CIE interval (with PC3 explaining 10.5% of the variance in this interval) hints at sulfides and/or other Hg sinks, such as (S-rich) OM, hosting the sedimentary Hg, evidencing a difference in the dominant host or carrier of Hg between the pre– and post–T-OAE negative CIE intervals.

Analysis of the T-OAE negative CIE interval itself shows that despite the dominant lithological control on total variance (PC1: 48.2%), Hg is also associated with sulfur (S) and HI, with a strong opposite negative loading for silicon (Si; PC2: explains 13.1% of total variance). This elemental association suggests that sedimentary Hg in this interval is hosted in marine OM (with HI values up to ~300 mg of hydrocarbons (HC)/g of TOC) and/or sulfides (Fig. 3 and fig. S2). Within the T-OAE negative CIE interval, raw sedimentary Hg concentrations also show a converse relationship to $\delta^{13}C_{TOC}$ (Fig. 2). This geochemical pattern further suggests that Hg during this time interval was being sequestered by marine OM (with elevated HI and more negative $\delta^{13}C_{TOC}$).

nMDS broadly supports the inference that lithological variation (carbonate dilution) predominantly explains the variance within the combined dataset. nMDS for the entire interval associates Hg with Al, K, Ti, and V (among others) versus Ca, Sr, TOC, and HI (Fig. 3), inferring a potential role for clays and sulfides in the shuttling and deposition of Hg. Combined, the PCA and nMDS analyses converge to suggest that the sedimentary association of Hg within the T-OAE negative CIE interval is different from the pre– and post–T-OAE negative CIE intervals.

Sedimentary Hg concentrations normalized against changes in (i) OM source (as reflected by changes in TOC and HI), (ii) detrital sediment supply (as reflected by Al and the kaolinite/illite ratio), and (iii) minor water column redox changes (as reflected by S, Fe, and V) do suggest above-background (or excess) Hg loading of the environment

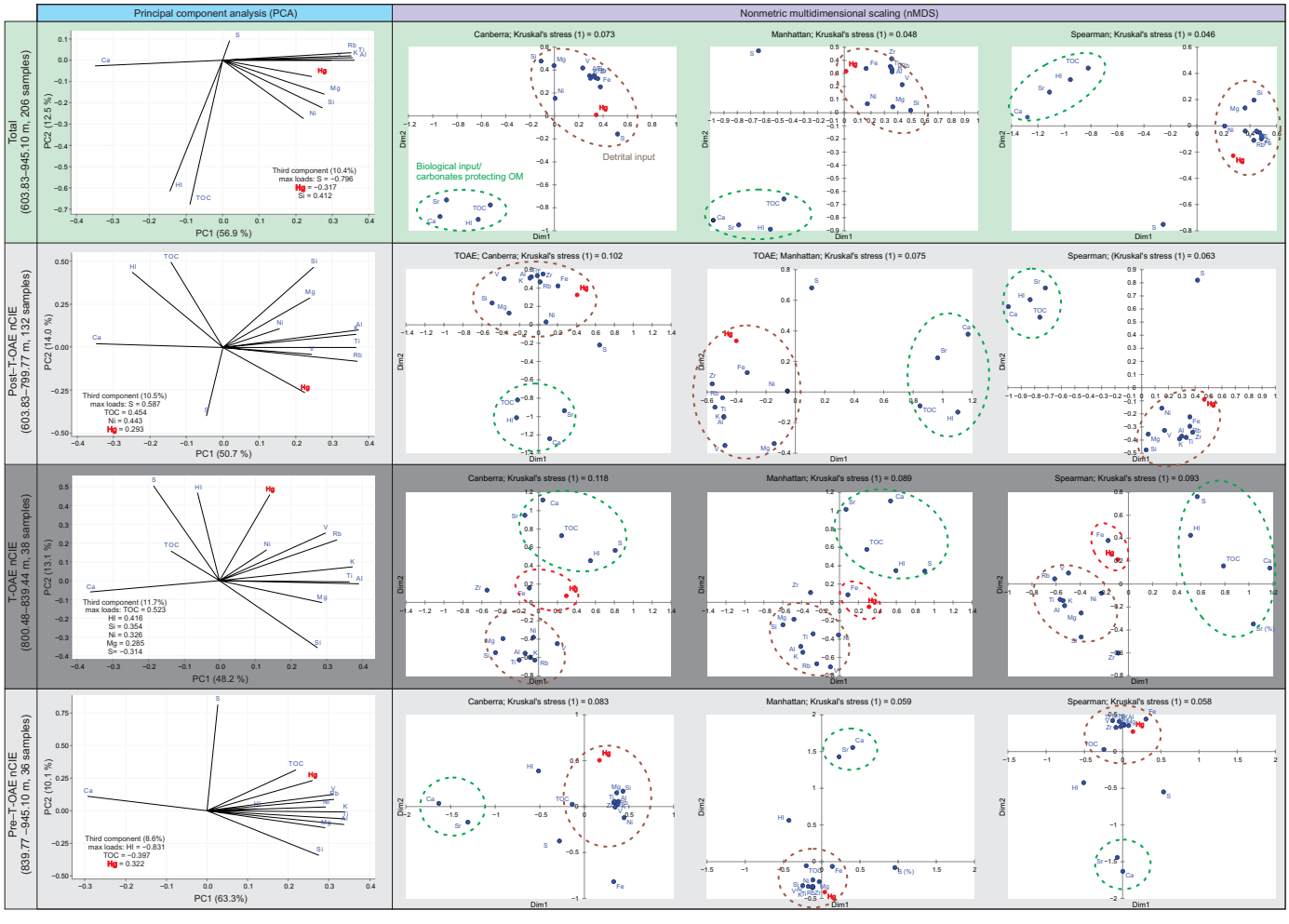

Fig. 3. Statistical analyses of the association of sedimentary Hg with other sedimentary geochemical proxies. PCAs and nMDS of the combined dataset, comprising the combined sedimentary geochemical parameters of the Upper Pliensbachian and entire Toarcian succession of the Mochras core, as well as stratigraphic subdatasets, showing the relative associations of sedimentary Hg with other parameters.

during the T-OAE negative CIE interval (fig. S2). The different sedimentary associations of Hg in the T-OAE negative CIE interval, concurrent with the "excess" Hg (when normalized), suggest that higher environmental Hg loading during the T-OAE negative CIE resulted in disproportionately higher Hg contents of clays, OM, and sulfides compared to preceding and succeeding time intervals. Alternatively, sedimentary Hg in the T-OAE negative CIE interval may have been associated with additional (unresolved) Hg hosts.

Whether Hg entered the Cardigan Bay Basin as aerosol air-fall from the atmosphere and/or through run-off from nearby landmasses is not yet fully constrained. However, in contrast to previous suggestions (*40*, *41*, *45*), it is apparent that no one single pathway dominated Hg sequestration during the Late Pliensbachian and Toarcian in the Cardigan Bay Basin. Elevated sedimentary Hg levels coinciding with the CIEs associated with the T-OAE in the Mochras core are therefore inferred to have resulted from excess environmental loading of Hg, likely sourced from enhanced Karoo-Ferrar volcanism.

DISCUSSION

Age and duration of Karoo-Ferrar LIP magmatism

The temporal and causal links between LIP volcanism, associated carbon degassing, and the Early Toarcian carbon cycle and climatic and environmental perturbations are widely studied, but evidence to date has been largely circumstantial because of uncertainties in stratigraphic correlation between continental and marine sedimentary archives of Toarcian environmental change and terrestrial basalt emplacement. Although paleomagnetic and geochronological age determinations of sedimentary deposits and basalt emplacement at that time overlap within geological and analytical uncertainties (*5*, *23*, *50*), they do not provide any measure of variations in the magnitude of volcanic activity at that time.

Our study of Early Toarcian changes in sedimentary Hg concentrations extends other datasets (*14*, *25*) and may, within the constraints and uncertainties described above, reflect variations in the magnitude of major Early Toarcian magmatism. Furthermore, the sedimentary Hg record of the bio-, magneto-, and chemostratigraphically calibrated Mochras core presented here, spanning the upper Pliensbachian and entire Toarcian stages, provides the first record of Early Toarcian enrichments in sedimentary Hg levels in a long-term context. The new record allows for the first assessment on the duration and age of peak Hg levels and, by inference, peak magmatism. The data presented here suggest a prolonged ~3-Ma period of elevated environmental Hg fluxes, in response to extended, elevated magmatic activity, from the Pliensbachian–Toarcian boundary, at ~184.2 Ma, to the onset of the *bifrons* zone, at ~181.2 Ma, thus with LIP magmatism occurring for over ~3 Ma (Fig. 2). However, changes in Hg sequestration pathways through time in the Cardigan Bay Basin over this interval may have enhanced the relative Hg concentrations and Hg/TOC ratios, particularly in the earliest Toarcian (see above). Because of these complications, the most elevated sedimentary Hg enrichments and, by inference, peak environmental Hg loading from peak magmatism occurred for a shorter period of time, from the latest *tenuicostatum* zone to the early *serpentinum* zone (lower half of the *exaratum* subzone; Fig. 2). Peak sedimentary Hg enrichment directly coincides with the onset and main phase of the Early Toarcian negative CIE, which is superimposed on the long-term Pliensbachian-Toarcian positive CIE, representing the time of net excess carbon release, lasting for 10^5 to 10^6 years [(*2*) and references therein]. Widespread elevated sedimentary Hg concentrations at this time suggest globally elevated environmental Hg fluxes through atmospheric dispersal. Although the data presented here invoke a volcanic source for the Hg, through volcanic degassing into the atmosphere, some of the Hg may have been volatilized through thermal maturation of subsurface organic-rich deposits intruded by Karoo-Ferrar–associated dikes and sills. This latter mechanism may explain the close temporal link between elevated Hg fluxes and the major negative shift in the $\delta^{13}C$ composition of Earth's surficial carbon pools, for which thermogenic methane release may have been the predominant culprit (*3*, *4*, *51*).

Reduced plate motion–controlled timing of Karoo-Ferrar LIP magmatism and the T-OAE

The Karoo-Ferrar LIP was emplaced as extrusive basalt with associated dikes and sills, with outcrop, borehole, and seismic data reflecting a present-day extent that covers southern Africa (Karoo), Antarctica (Ferrar), and Australasia (Ferrar) (*5*, *22*, *52*–*59*). The U-Pb, $^{40}Ar/^{39}Ar$, and K-Ar radio-isotopic dates for the Karoo-Ferrar tholeiitic basalts and dolerites suggest a short period of formation, with most of the magmatic emplacement occurring within a <1-Ma window centered around ~182.7 Ma, across a paleogeographic distance of ~6000 km (Fig. 1) (*5*, *22*, *56*). Individual magmatic bodies were possibly, however, emplaced over more extended time intervals, such as the >1500-m-thick basalt accumulation in Lesotho (*23*, *58*).

The mechanism for the coeval emplacement of the Karoo and Ferrar LIP components is much debated and stems from differences in the (trace) elemental compositions that reflect mid ocean ridge basalt (MORB) or plume versus mixed plume–subduction geochemical signatures [(*57*, *60*) and references therein]. Subduction of the Phoenix and Farallon plates underneath Pangea resulted in Mesozoic volcanic arcs and back-arc basins along the western margin of present-day South America. Deep subduction of the Phoenix Plate has been suggested as a dehydrated magma source for Ferrar magmatic rocks [(*57*) and references therein]. Although the former Phoenix and continental Pangean plate boundary directly bordered the Mesozoic volcanic arcs in present-day Chile and Argentina in the late Early Jurassic, the boundary was located 2000 to 5000 km west/southwest of the nearest recorded Karoo-Ferrar LIP igneous activity (Fig. 1). Furthermore, the MORB signatures of particularly Karoo (and possibly Ferrar) rocks suggest a likely role for mantle plumes in LIP emplacement at that time.

Mantle plumes in this region are suggested to have originated from the plume generation zone near the core-mantle boundary associated with the African large low shear velocity province (LLSVP) (*61*–*64*). Many Phanerozoic LIPs appear to have formed associated with LLSVP margins, especially when LLSVPs were overlain by supercontinents, linking core-mantle boundary processes, plume generation, and Earth's surficial processes (*61*).

Irrespective of the source of mantle plumes, it is commonly hypothesized that when the plume head reaches the base of the lithosphere below a craton, it gradually thermally erodes it (both the uppermost solid mantle and brittle crust), followed by dike and sill intrusions into possibly overlying subsurface sedimentary deposits, and ultimately, surface basalt emplacement (*65*, *66*).

Using comprehensive plate model reconstructions of [(*67*) and references therein], here imaged using GPlates (*68*), we show that timing of Early Toarcian LIP emplacement is not best explained by the arrival of a plume head at the base of the Southern Pangean cratonic

lithosphere but rather by a substantial and prolonged reduction in plate motion before LIP emplacement and associated with a reduction in plate velocity preceding a reversal in plate movement direction, through which an existing plume head was effectively allowed to thermally erode and penetrate the temporarily near-static overlying craton.

The plate model reconstruction used here adopts the true polar wander–corrected paleomagnetic reference frame of (*69*) from 230 to 100 Ma [with a 10° westward longitudinal shift to correct for mismatches between mantle structures and associated surface geology: see (*67*)], and the global moving hot spot reference frame of (*64*, *70*), from 70 to 0 Ma. This shows the absolute plate motion of the southern Pangean continent (i.e., South America, Africa, Antarctica, and Australasia) changing direction from predominantly north to largely south in the late Early Jurassic (Fig. 1), with a gradual reduction to a near-zero (<2 cm/year) rate of plate velocity over both the Tristan Da Cunha and Bouvet hot spots in the late Early Jurassic from Late Triassic plate velocities of ~8 cm/year (Fig. 1) (*71*). Uncertainties on plate positions and velocities for times for which oceanic crustal/seafloor records (and associated seafloor spreading anomalies or age-progressive hot spot trails) no longer exist are alleviated by paleomagnetic data constraining absolute plate motions and onshore geological data constraining relative plate motions (e.g., dating of geological substrates indicative of past plate convergence/subduction zones). With these data, the age and geographical uncertainty on relative and absolute plate movements and rotations in the Mesozoic, as reconstructed here in GPlates, are relatively minor (up to a few million years and few degrees latitude and longitude) (*67*, *72*). The absolute reference frame for Pangea assumes no longitudinal movement for the African Plate (*69*). Furthermore, reconstructed plate velocities are sensitive to the absolute reference frame used (*71*, *72*), accentuating temporal peaks or troughs in global plate velocity records. Crucially, alternative reference frames based on tomographically derived inferences of past subduction (*73*) equally show a substantial reduction in the velocity of the African (and global continental) plate(s) in the late Early Jurassic [www.paleolatitude.org (*74*)]. With these factors combined, we determine that, during the late Early Jurassic, the Tristan Da Cunha and Bouvet hot spots directly or closely underlay the Karoo and Ferrar igneous centers, respectively, and that Karoo and Ferrar magmatic emplacements temporally coincided with a reduction in plate motion and the inferred reversal in plate movement direction, and an associated period of near-zero plate velocity (Fig. 1). This temporal link, combined with the late Early Jurassic geographical proximity of the Tristan Da Cunha and Bouvet hot spots, suggests a causal relationship in which plume head magmas were only effective in thermally eroding and penetrating the overriding craton after a prolonged reduction in plate motion, effectively when plate movement had reduced to (virtually) zero (Figs. 1 and 4). The similarity in plate motion evolution of the African and Antarctic cratons overlying the Tristan Da Cunha and Bouvet hot spot localities, respectively, may

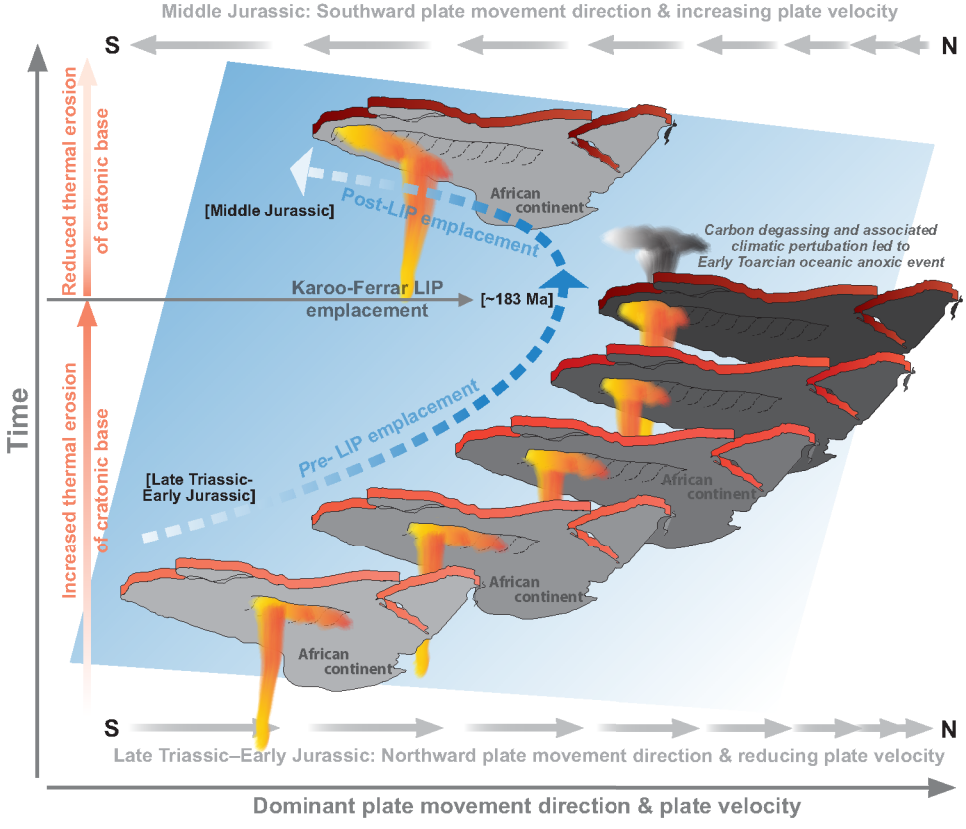

Fig. 4. Conceptual model linking changes in plate motion with surface magmatism. Conceptual model (showing the African continent viewed from below) linking a reduced plate velocity with increased effectiveness of underlying mantle-plume magmas to thermally erode the mantle and crustal lithosphere, leading to the emplacement of the Karoo-Ferrar LIP in Southern Pangea (southern African craton), at ~183 Ma, concurrently with a reversal in plate movement direction. Subsequently, increased local plate velocities led to the mantle plume increasingly being overlain by thermally non-eroded crustal lithosphere, ending the surficial hot spot activity and LIP magmatism.

explain why the geochemically different and geographically separated Karoo and Ferrar LIPs were emplaced at almost the same time (*5*, *50*), with reduced plate motion rather than plume head arrival controlling the timing of LIP emplacement from possibly two separate mantle plumes.

Southern Pangea returned to earlier rates of plate motion in the late Toarcian, with plate velocity increasing back to ~8 cm/year, soon after the reversal in plate movement direction. The associated shift in the relative position of the hot spot to underlie thicker, previously non-eroded parts of the craton then hypothetically limited the duration of surficial Karoo-Ferrar LIP magmatism to ~3 Ma (Fig. 1). Peak surficial volcanic activity diminished in the middle Toarcian *bifrons* zone (section 4), as evidenced by the end to carbon cycle disruption and carbon and Hg degassing, when plate velocities reached >2 cm/year, halting further substantial basaltic igneous activity (Figs. 1 and 4).

LIPs across the African and Arabian cratons, attributed to deep mantle plumes, generally appear to have been formed at localities where the base of the lithosphere was concurrently lost because of thermal erosion, implying that mantle plumes can actively cause cratonic roots to founder by thinning the overlying mantle and crustal lithosphere when given enough time (*66*).

Waveform tomography suggests that the base of the lithosphere beneath southern Africa is fragmented and separated by troughs, likely caused, at least in part, by prolonged and widespread lithospheric erosion over the past 200 Ma by the Tristan Da Cunha hot spot (*66*). Prolonged erosion of the base of the cratonic lithosphere before emplacement of Karoo and Ferrar magmatic bodies may explain the lithospheric geochemical signature that partly characterizes their basaltic composition (*60*).

Deep mantle plumes, considered as sourced from the deep mantle or core-mantle boundary, may be one to three orders of magnitude enriched in carbon relative to the upper mantle (*75*, *76*). An increased carbon content in mantle plume-derived magmatic rocks, relative to MORB, for example, suggests that major plume-sourced volcanic events, such as the Karoo-Ferrar LIP, may have been accompanied by much higher fluxes of (isotopically light) magmatic carbon degassing than previously estimated (*77*). This phenomenon, combined with the carbon degassing from dike- and sill-intruded subsurface (organic-rich) sediments (*4*, *78*) and the possible initiation of positive feedback loops in the global climate system leading to methane release from ocean-floor clathrates and/or terrestrial cryogenic environments (*3*, *79*–*81*), may explain the highly negative $\delta^{13}C$ values of marine and terrestrial substrates and, by implication, the atmosphere and ocean at this time despite concomitant widespread and photosynthetically derived (isotopically light) organic carbon sequestration that is the primary hallmark of the T-OAE. In addition, plume-lithosphere interactions may also have released large quantities of halogens into the atmosphere at this time, potentially causing acid rain and increasing the flux of toxic compounds into the environment, further affecting ecosystem stability.

After Early Jurassic magmatism in the Karoo region ceased, the Tristan Da Cunha hot spot only reemerged as a source for surficial basalt emplacement with the development of the Paraná-Etendeka LIP at 134 Ma and the formation of the Walvis Ridge, associated with the opening of the South Atlantic and the westward movement of Africa that allowed the hot spot to "reappear" from below the South African craton (*82*). This observation supports the notion that a moving craton overlying an active mantle plume does actively halt surficial basalt emplacement by temporally limiting the thermal erosion of the cratonic lithosphere. Crucially, even when multiple mantle plumes were generated from the plume generation zone associated with the African LLSVP and even when these mantle plumes individually gave rise to southern and southwestern African magmatism in the Early Jurassic (Karoo), the Early Cretaceous (Paraná-Etendeka), and Cenozoic (Walvis Ridge), changes in overlying plate motion would likely still have controlled the timing of surficial LIP emplacement, following the model presented here.

Plate motion control on other LIP emplacements

Continental plate movement control on the timing of continental LIP emplacement, as here proposed for the Karoo-Ferrar LIP, may have been a common mechanism throughout much of Earth history. For example, the Siberian Traps formed over 2 to 3 Ma, with an early onset at ~252 Ma, across the West Siberian Basin and the Noril'sk and Tunguska regions of the Siberian Craton, and this LIP has been widely accepted as the instigator of the end-Permian mass extinction [at ~251.9 Ma (*83*, *84*)]. The West Siberian Basin and Siberian Craton migrated substantially through the Late Paleozoic, with the plate reconstruction model used here suggesting a ~15° shift east and north from 300 Ma onward (Fig. 5A). This prolonged migration pathway was abruptly interrupted by a substantial reduction in local plate motion from ~260 Ma onward, and a reduction to near-zero plate velocities leading up to a reversal in plate movement direction from northeast to west-northwest at ~252 Ma (Fig. 5A), directly coinciding with the onset of the Siberian Traps formation. Local plate velocities remained near zero until ~249 Ma, coinciding with the main window of Siberian Traps emplacement, after which the local plate velocity again increased and LIP volcanism ceased. Even when considering the larger longitudinal uncertainty on the plate reconstruction model used here, this suggests that a reduction in local plate motion also contributed to controlling the timing of emplacement of the Siberian Traps, one of the largest LIPs on Earth, and, consequently, the timing of the end-Permian mass extinction, the largest such event in Earth history.

In the Mesozoic and Early Cenozoic, the Greenland craton underwent a substantial migration from east to west over the Iceland hot spot, from ~90 to 60 Ma, leaving a thermally eroded corridor of thinned lithosphere across the Central Greenland craton (*65*). The thick Greenland craton, combined with its plate velocity, prohibited a hot spot track from forming but accumulated plume magmas spread through this lithospheric corridor. The plate reconstruction model used here suggests that also the emergence of the Iceland hot spot from under Greenland's east coast, after the craton had migrated westward, instigated (together with nearby mid-ocean spreading ridges) basalt emplacement, leading to the onset and first phase of North Atlantic Igneous Province volcanism at ~60 Ma (Fig. 5B) (*65*, *85*), followed by a second phase of magmatism at ~56 Ma, possibly causing the Paleocene-Eocene Thermal Maximum (*28*, *86*). These observations may suggest that the migration and velocity of the Greenland craton initially effectively suppressed the surface expression of the Iceland Plume, with a hot spot track only forming when the thick cratonic lithosphere migrated away to make room for thinner proto-oceanic crust.

A major control of plate movement and velocity on surficial LIP emplacement is possibly further exemplified by the long emplacement history of the mantle plume–derived African-Arabian LIP (*87*), concomitant with the prolonged relatively static position of

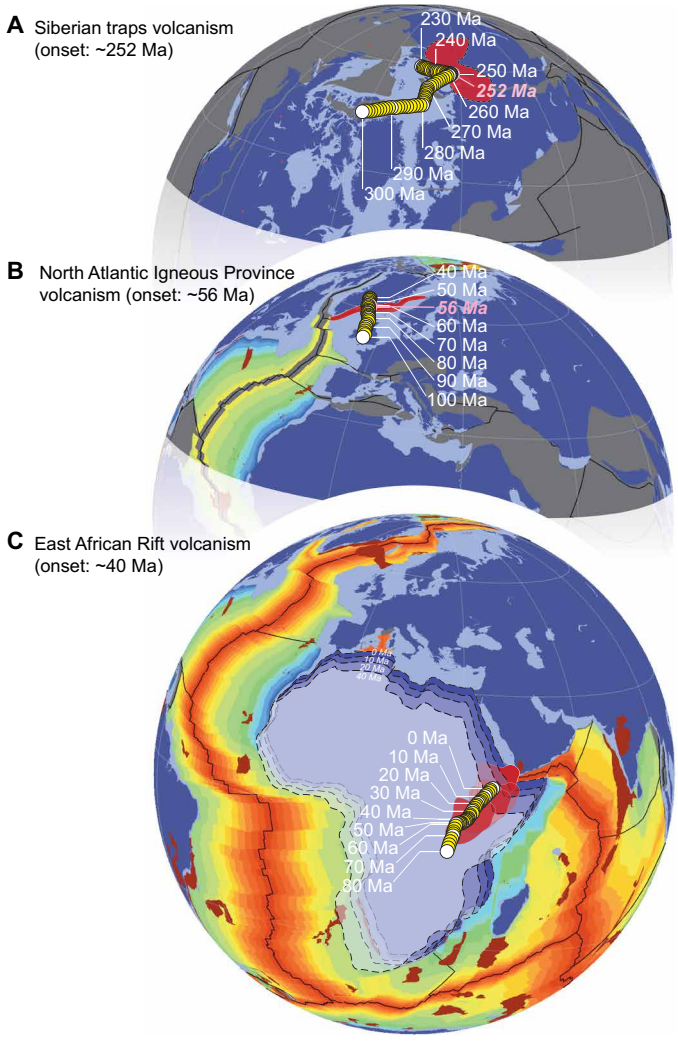

Fig. 5. Paleo-, Meso-, and Cenozoic changes in plate motion and their impact on the relative position of hot spots. Paleo-, Meso-, and Cenozoic examples of possible local plate velocity control on the timing (onset, duration, and continuation) of LIP magmatism overlying mantle plumes. (**A**) The onset of Siberian Traps emplacement coincided with a near-zero local plate velocity and a reversal in local plate movement direction at ~252 Ma, with the duration of LIP emplacement being concurrent with a prolonged near-zero local plate velocity. (**B**) The onset of North Atlantic Igneous Province LIP volcanism at ~56 Ma coincided with the "emergence" of the Iceland Plume from underneath the Greenland craton, following the latter's prolonged westward movement for the preceding 30 Ma. (**C**) The onset of East African Rift volcanism temporally coincided with a substantial reduction to near zero in the local plate velocity. The reduction to a near-zero local plate velocity possibly instigated surficial magmatism from the underlying mantle plume(s), and the continued, reduced local plate velocity possibly enabled continued magmatism locally throughout the Late Cenozoic.

the African plate throughout the Late Cenozoic. Substantial debate exists on the nature and origin of magmatism in the East African rift region, with competing models for a super-plume, multiplume, or smaller igneous centers (*87*–*91*). The plate reconstruction model used here suggests that the African craton has rotated counterclockwise by a few degrees, with only a minor 15° northward migration of Eastern Africa over the past 80 Ma. However, local plate motion and velocity have been highly variable over this time period, with, on average, ~4 cm/year of northward drift from 80 to 60 Ma, a reduced ~2 cm/year northward drift from 35 to 0 Ma, and a minor 0.5 to 1 cm/year northward drift from 60 to 35 Ma (Fig. 5). The latter period of prolonged reduction in plate motion, combined with a superimposed near-zero local plate velocity at ~40 Ma (Fig. 5), coincides with the early onset of volcanism in the Southern Ethiopian rift region. This was followed by a later onset of magmatism in the Kenya/Tanzania dome region (*92*) as the East African craton migrated further northward. This temporal and spatial transect in the onset of magmatism, possibly due to the northward migration of East Africa over a mantle plume, occurred in line with the north-to-south evolution of basalt and noble gas geochemistry, which both suggest MORB signatures for present-day volcanism in the Ethiopia/Afar region but with more of a crustal mixing signature in the younger Kenyan Dome region (*87*). The data suggest an explanation in which a plate with a prolonged reduction in plate motion and an associated near-zero local plate velocity overlying a mantle plume allowed for thermal processes to erode the base of the cratonic lithosphere sufficiently to initiate surficial magmatism, followed by prolonged and continued basalt emplacement when the craton continued to migrate northward at only low velocities (Fig. 5).

The Siberian Traps, the Karoo-Ferrar, the North Atlantic Igneous Province, and the East African Rift LIP regions all show a substantial reduction in local plate velocities and an associated reduction in local total plate movement in the millions of years leading up to LIP emplacement (Fig. 5) (*65*), allowing locally for a prolonged buildup of plume-derived magmas and thermal erosion of the cratonic lithosphere and subsequent emplacement of the LIPs. Although the timing of emplacement of other continental LIPs (such as the Central Atlantic Magmatic Province) may have equally been forced by changes in local plate motion, the timing of a temporary reduction in local plate velocity at these times is currently difficult to establish with certainty because of the predominantly longitudinal direction of local plate movement and the greater uncertainties in the model used here to establish the past longitudinal plate positions.

In conclusion, understanding how solid Earth processes drive changes in our planet's surface environment is important in understanding planetary evolution. The study of sedimentary Hg concentrations in the bio-, chemo-, and paleomagnetically constrained and stratigraphically expanded Lower Jurassic sedimentary archive of the Mochras borehole (Cardigan Bay Basin, UK) shows substantial Hg enrichments and Hg/TOC ratios from the Pliensbachian-Toarcian boundary up to the base of the *bifrons* zone, spanning ~3 Ma of the Early Toarcian, including the T-OAE. These observations suggest prolonged volcanic activity, likely associated with Karoo-Ferrar LIP volcanism, leading to a prolonged period of elevated environmental Hg loading and enhanced fluxes into the global sedimentary record. PCAs, combined with nMDS of sedimentary Hg and other geochemical proxy records from the same core, however, suggest temporal variations in the dominant Hg sequestration pathways in the Cardigan Bay Basin, from the Late Pliensbachian through to the Late Toarcian. Because of these fluctuations, peak environmental Hg fluxes and, by inference, peak magmatic activity likely occurred over a shorter period of time, directly coinciding with the T-OAE negative CIE, at ~183 Ma.

The analysis of temporal variations in reconstructed Late Triassic and Early Jurassic plate motions shows that the Karoo-Ferrar region experienced a prolonged period of reducing plate motion, culminating in a virtually zero plate velocity (compared to ~8 cm/year

before and after) at ~183 Ma, and a subsequent shift in plate movement direction, from predominantly north to predominantly south.

Changes in plate movement direction and associated reductions in local plate velocities appear temporally and spatially linked to the emplacement of some of the largest Paleozoic, Mesozoic, and Cenozoic LIP events (such as the Permian–Triassic Siberian Traps, the Paleocene–Eocene North Atlantic Igneous Province, and the Paleogene and Neogene East African Rift Basalts), suggesting an as-yet unexplored control on the onset, timing, and demise of emplacement of major continental LIPs and the associated cascade of global change events instigated by the degassing of carbon and toxic compounds and the initiation or enhancement of climate feedbacks at these times.

Thermal erosion of the overriding cratonic lithosphere by deep mantle plumes may only have been effective in intruding the lithosphere and crust and emplacing a LIP when enough time was permitted for these processes to occur because of low or reduced overriding plate velocities and a prolonged, reduced plate motion.

This model implies that global plate tectonic processes, rather than plume head arrival, are an important root cause for the onset and demise of continental LIP emplacement throughout Earth history. Hence, the associated carbon degassing, the timing and duration of global climatic and environmental perturbations, ecosystem disruption, and mass extinction together illustrate the mechanistic linkage between the internal and surficial processes of the Earth system.

MATERIALS AND METHODS

Sedimentary mercury analyses and ordination (principal component and nMDS)

A suite of 400 rock samples was selected from the Mochras core, from 948.15 m (upper Pliensbachian *margaritatus* zone, *subnodosus-gibbosus* subzones) to 602.06 m (uppermost Toarcian *aalensis* zone). Samples were analyzed for their major and minor elemental concentrations, mineral composition, TOC content, HI, and carbon-isotopic composition of OM ($\delta^{13}C_{TOC}$), as reported in (*7*, *8*). The Hg content of samples reported here was analyzed at the Earth Surface Research Laboratory of the Department of Geology, Trinity College Dublin, The University of Dublin using a LECO AMA-254 Mercury analyzer, following the methodology described in (*93*), and at the Department of Earth Sciences, University of Oxford using a RA-915 Portable Mercury Analyzer with PYRO-915 Pyrolyzer, Lumex [as described in (*94*)] (see the Supplementary Materials for further details). The combined Mochras dataset was interrogated using two different ordination methods: PCA was performed using Minitab software (version 19.2020), and nMDS was performed using XLSTAT (version 2021.1.1), on both the entire dataset, as well as specific stratigraphic subsets [pre–T-OAE negative CIE (603.83 to 799.77 m, 132 samples), T-OAE negative CIE (800.48 to 839.44 m, 38 samples), and post–T-OAE negative CIE (839.77 to 945.10 m, 36 samples); see the Supplementary Materials for further details].

SUPPLEMENTARY MATERIALS

Supplementary material for this article is available at https://science.org/doi/10.1126/sciadv.abo0866

REFERENCES AND NOTES

1. H. C. Jenkyns, Geochemistry of oceanic anoxic events. *Geochem. Geophys. Geosyst.* **11**, Q03004 (2010).
2. S. P. Hesselbo, J. G. Ogg, M. Ruhl, The Jurassic Period, in *Geologic Time Scale 2020*, F. M. Gradstein, J. G. Ogg, M. D. Schmitz, G. M. Ogg, Eds. (Elsevier, 2020), pp. 955–1021.
3. S. P. Hesselbo, D. R. Gröcke, H. C. Jenkyns, C. J. Bjerrum, P. Farrimond, H. S. Morgans Bell, O. R. Green, Massive dissociation of gas hydrate during a Jurassic oceanic anoxic event. *Nature* **406**, 392–395 (2000).
4. J. C. McElwain, J. Wade-Murphy, S. P. Hesselbo, Changes in carbon dioxide during an oceanic anoxic event linked to intrusion into Gondwana coals. *Nature* **435**, 479–482 (2005).
5. S. D. Burgess, S. A. Bowring, T. H. Fleming, D. H. Elliot, High-precision geochronology links the Ferrar large igneous province with early-Jurassic ocean anoxia and biotic crisis. *Earth Planet. Sci. Lett.* **415**, 90–99 (2015).
6. H. C. Jenkyns, C. E. Jones, D. R. Gröcke, S. P. Hesselbo, D. N. Parkinson, Chemostratigraphy of the Jurassic system: Applications, limitations and implications for palaeoceanography. *J. Geol. Soc. Lond.* **159**, 351–378 (2002).
7. W. Xu, M. Ruhl, H. C. Jenkyns, M. J. Leng, J. M. Huggett, D. Minisini, C. V. Ullmann, J. B. Riding, J. W. H. Weijers, M. S. Storm, L. M. E. Percival, N. J. Tosca, E. F. Idiz, E. W. Tegelaar, S. P. Hesselbo, Evolution of the Toarcian (Early Jurassic) carbon-cycle and global climatic controls on local sedimentary processes (Cardigan Bay Basin, UK). *Earth Planet. Sc. Lett.* **484**, 396–411 (2018a).
8. M. S. Storm, S. P. Hesselbo, H. C. Jenkyns, M. Ruhl, C. V. Ullmann, W. Xu, M. J. Leng, J. B. Riding, O. Gorbanenko, Orbital pacing and secular evolution of the Early Jurassic carbon cycle. *Proc. Natl. Acad. Sci. U.S.A.* **117**, 3974–3982 (2020).
9. J. J. Gómez, A. Goy, Warming-driven mass extinction in the Early Toarcian (Early Jurassic) of northern and central Spain. Correlation with other time-equivalent European sections. *Palaeogeogr. Palaeoclimatol. Palaeoecol.* **306**, 176–195 (2011).
10. W. Ruebsam, M. Reolid, L. Schwark, $\delta^{13}C$ of terrestrial vegetation records Toarcian CO_2 and climate gradients. *Sci. Rep.* **10**, 117 (2020).
11. C. V. Ullmann, R. Boyle, L. V. Duarte, S. P. Hesselbo, S. A. Kasemann, T. Klein, T. M. Lenton, V. Piazza, M. Aberhan, Warm afterglow from the Toarcian oceanic anoxic event drives the success of deep-adapted brachiopods. *Sci. Rep.* **10**, 6549 (2020).
12. B. Hönisch, A. Ridgwell, D. N. Schmidt, E. Thomas, S. J. Gibbs, A. Sluijs, R. Zeebe, L. Kump, R. C. Martindale, S. E. Greene, W. Kiessling, J. Ries, J. C. Zachos, D. L. Royer, S. Barker, T. M. Marchitto Jr., R. Moyer, C. Pelejero, P. Ziveri, G. L. Foster, B. Williams, The geological record of ocean acidification. *Science* **335**, 1058–1063 (2012).
13. T. Müller, H. Jurikova, M. Gutjahr, A. Tomašových, J. Schlögl, V. Liebetrau, L. V. Duarte, R. Milovský, G. Suan, E. Mattioli, B. Pittet, A. Eisenhauer, Ocean acidification during the early Toarcian extinction event: Evidence from boron isotopes in brachiopods. *Geology* **48**, 1184–1188 (2020).
14. L. M. E. Percival, A. S. Cohen, M. K. Davies, A. J. Dickson, S. P. Hesselbo, H. C. Jenkyns, M. J. Leng, T. A. Mather, M. S. Storm, W. Xu, Osmium isotope evidence for two pulses of increased continental weathering linked to Early Jurassic volcanism and climate change. *Geology* **44**, 759–762 (2016).
15. S. J. Baker, S. P. Hesselbo, T. M. Lenton, L. V. Duarte, C. M. Belcher, Charcoal evidence that rising atmospheric oxygen terminated Early Jurassic ocean anoxia. *Nat. Commun.* **8**, 15018 (2017).
16. T. R. Them II, B. C. Gilla, A. H. Caruthers, D. R. Gröckee, E. T. Tulskya, R. C. Martindale, T. P. Poulton, P. L. Smith, High-resolution carbon isotope records of the Toarcian oceanic anoxic event (Early Jurassic) from North America and implications for the global drivers of the Toarcian carbon cycle. *Earth Planet. Sci. Lett.* **459**, 118–126 (2017).
17. W. Xu, M. Ruhl, H. C. Jenkyns, S. P. Hesselbo, J. B. Riding, D. Selby, B. D. A. Naafs, J. W. H. Weijers, R. D. Pancost, E. W. Tegelaar, E. F. Idiz, Carbon sequestration in an expanded lake system during the Toarcian oceanic anoxic event. *Nat. Geosci.* **10**, 129–134 (2017).
18. S. M. Slater, R. J. Twitchett, S. Danise, V. Vajda, Substantial vegetation response to Early Jurassic global warming with impacts on oceanic anoxia. *Nat. Geosci.* **12**, 462–467 (2019).
19. R. L. Silva, M. Ruhl, C. Barry, M. Reolid, W. Ruebsam, Pacing of late Pliensbachian and early Toarcian carbon cycle perturbations and environmental change in the westernmost Tethys (La Cerradura Section, Subbetic zone of the Betic Cordillera, Spain). *Geol. Soc. Spec. Publ.* **514**, 387–408 (2021).
20. P. B. Wignall, R. J. Newton, C. T. S. Little, The timing of paleoenvironmental change and cause-and-effect relationships during the Early Jurassic mass extinction in Europe. *Am. J. Sci.* **305**, 1014–1032 (2005).
21. C. V. Ullmann, N. Thibault, M. Ruhl, S. P. Hesselbo, C. Korte, Effect of a Jurassic oceanic anoxic event on belemnite ecology and evolution. *Proc. Natl. Acad. Sci. U.S.A.* **111**, 10073–10076 (2014).
22. B. Sell, M. Ovtcharova, J. Guex, A. Bartolini, F. Jourdan, J. E. Spangenberg, J. C. Vicente, U. Schaltegger, Evaluating the temporal link between the Karoo LIP and climatic–biologic events of the Toarcian Stage with high-precision U–Pb geochronology. *Earth Planet. Sci. Lett.* **408**, 48–56 (2014).
23. W. Xu, C. M. Niocaill, M. Ruhl, H. C. Jenkyns, J. B. Riding, S. P. Hesselbo, Magnetostratigraphy of the Toarcian Stage (Lower Jurassic) of the Llanbedr (Mochras Farm) Borehole, Wales: Basis for a global standard and implications for volcanic forcing of palaeoenvironmental change. *J. Geol. Soc. London* **175**, 594–604 (2018b).

24. D. M. Pyle, T. A. Mather, The importance of volcanic emissions for the global atmospheric mercury cycle. *Atmos. Environ.* **37**, 5115–5124 (2003).
25. L. M. E. Percival, M. L. I. Witt, T. A. Mather, M. Hermoso, H. C. Jenkyns, S. P. Hesselbo, A. H. Al-Suwaidi, M. S. Storm, W. Xu, M. Ruhl, Globally enhanced mercury deposition during the end-Pliensbachian and Toarcian OAE: A link to the Karoo–Ferrar large igneous province. *Earth Planet. Sci. Lett.* **428**, 267–280 (2015).
26. L. M. E. Percival, M. Ruhl, S. P. Hesselbo, H. C. Jenkyns, T. A. Mather, J. H. Whiteside, Mercury evidence for pulsed volcanism during the end-Triassic mass extinction. *Proc. Natl. Acad. Sci. U.S.A.* **114**, 7929–7934 (2017).
27. H. Sanei, S. E. Grasby, B. Beauchamp, Latest Permian mercury anomalies. *Geology* **40**, 63–66 (2012).
28. M. T. Jones, L. M. E. Percival, E. W. Stokke, J. Frieling, T. A. Mather, L. Riber, B. A. Schubert, B. Schultz, C. Tegner, S. Planke, H. H. Svensen, Mercury anomalies across the Palaeocene–Eocene thermal maximum. *Clim. Past* **15**, 217–236 (2019).
29. E. B. Kovács, M. Ruhl, A. Demény, I. Fórizs, I. Hegyi, Z. R. Horváth-Kostka, F. Móricz, Z. Vallner, J. Pálfy, Mercury anomalies and carbon isotope excursions in the western Tethyan Csővár section support the link between CAMP volcanism and the end-Triassic extinction. *Glob. Planet. Change* **194**, 103291 (2020).
30. S. Lindström, S. Callegaro, J. Davies, C. Tegner, B. van de Schootbrugge, G. K. Pedersen, N. Youbi, H. Sanei, A. Marzoli, Tracing volcanic emissions from the Central Atlantic Magmatic Province in the sedimentary record. *Earth Sci. Rev.* **212**, 103444 (2021).
31. M. Ruhl, S. P. Hesselbo, A. al-Suwaidi, H. C. Jenkyns, S. E. Damborenea, M. O. Manceñido, M. Storm, T. A. Mather, A. C. Riccardi, On the onset of Central Atlantic Magmatic Province (CAMP) volcanism and environmental and carbon-cycle change at the Triassic–Jurassic transition (Neuquén Basin, Argentina). *Earth Sci. Rev.* **208**, 103229 (2020).
32. A. N. Sial, J. Chen, C. Korte, M. K. Pandit, J. Spangenberg, J. C. Silva-Tamayo, L. D. de Lacerda, V. P. Ferreira, J. A. Barbosa, C. Gaucher, N. S. Pereira, P. R. Riedel, Globally enhanced Hg concentration and Hg and C isotopes in Permian–Triassic boundary successions: Possible linkage to volcanism. *Stratigraphy Timescales* **5**, 567–628 (2020).
33. S. E. Grasby, T. R. Them II, Z. Chen, R. Yin, O. H. Ardakani, Mercury as a proxy for volcanic emissions in the geologic record. *Earth Sci. Rev.* **196**, 102880 (2019).
34. K. L. Bowmana, C. R. Hammerschmidt, C. H. Lamborg, G. Swarr, Mercury in the North Atlantic Ocean: The U.S. GEOTRACES zonal and meridional sections. *Deep-Sea Res. II Top. Stud. Oceanogr.* **116**, 251–261 (2015).
35. M. Liu, Q. Zhang, T. Maavara, S. Liu, X. Wang, P. A. Raymond, Rivers as the largest source of mercury to coastal oceans worldwide. *Nat. Geosci.* **14**, 672–677 (2021).
36. W. H. Schroeder, J. Munthe, Atmospheric mercury – An overview. *Atmos. Environ.* **32**, 809–822 (1998).
37. N. E. Selin, Global biogeochemical cycling of mercury: A review. *Annu. Rev. Env. Resour.* **34**, 43–63 (2009).
38. B. Hall, The gas phase oxidation of elemental mercury by ozone. *Water Air Soil Pollut.* **80**, 301–315 (1995).
39. S. E. Grasby, W. Shen, R. Yin, J. D. Gleason, J. D. Blum, R. F. Lepak, J. P. Hurley, B. Beauchamp, Isotopic signatures of mercury contamination in latest Permian oceans. *Geology* **45**, 55–58 (2017).
40. T. R. Them II, C. H. Jagoe, A. H. Caruthers, B. C. Gill, S. E. Grasby, D. R. Gröcke, R. Yin, J. D. Owens, Terrestrial sources as the primary delivery mechanism of mercury to the oceans across the Toarcian oceanic anoxic event (Early Jurassic). *Earth Planet. Sc. Lett.* **507**, 62–72 (2019).
41. J. D. Corso, B. J. W. Mills, D. Chu, R. J. Newton, T. A. Mather, W. Shu, Y. Wu, J. Tong, P. B. Wignall, Permo–Triassic boundary carbon and mercury cycling linked to terrestrial ecosystem collapse. *Nat. Commun.* **11**, 2962 (2020).
42. M. Ravichandran, Interactions between mercury and dissolved organic matter––A review. *Chemosphere* **55**, 319–331 (2004).
43. P. M. Outridge, L. H. Sanei, G. A. Stern, P. B. Hamilton, F. Goodarzi, Evidence for control of mercury accumulation rates in Canadian High Arctic lake sediments by variations of aquatic primary productivity. *Environ. Sci. Technol.* **41**, 5259–5265 (2007).
44. J. Shen, J. Chen, T. J. Algeo, S. Yuan, Q. Feng, J. Yu, L. Zhou, B. O'Connell, N. J. Planavsky, Evidence for a prolonged Permian-Triassic extinction interval from global marine mercury records. *Nat. Commun.* **10**, 1563 (2019).
45. J. Shen, Q. Feng, T. J. Algeo, J. Liu, C. Zhou, W. Wei, J. Liu, T. R. Them II, B. C. Gill, J. Chen, Sedimentary host phases of mercury (Hg) and implications for use of Hg as a volcanic proxy. *Earth Planet. Sci. Lett.* **543**, 116333 (2020).
46. S. E. Grasby, H. Sanei, B. Beauchamp, Z. Chen, Mercury deposition through the permo-triassic biotic crisis. *Chem. Geol.* **351**, 209–216 (2013).
47. L. M. E. Percival, H. C. Jenkyns, T. A. Mather, A. J. Dickson, S. J. Batenburg, M. Ruhl, S. P. Hesselbo, R. Barclay, I. Jarvis, S. A. Robinson, L. Woelders, Does large igneous province volcanism always perturb the mercury cycle? Comparing the records of oceanic anoxic event 2 and the end-Cretaceous to other Mesozoic events. *Am. J. Sci.* **318**, 799–860 (2018).
48. T. H. Heimdal, S. Callegaro, H. H. Svensen, M. T. Jones, E. Pereira, S. Planke, Evidence for magma–evaporite interactions during the emplacement of the Central Atlantic Magmatic Province (CAMP) in Brazil. *Earth Planet. Sci. Lett.* **506**, 476–492 (2019).
49. A. Menini, E. Mattioli, S. P. Hesselbo, M. Ruhl, G. Suan, Primary *versus* carbonate production in the Toarcian, a case study from the Mochras borehole (Wales). *Geol. Soc. Spec. Publ.* **514**, 59–81 (2021).
50. A. H. Al-Suwaidi, M. Ruhl, H. C. Jenkyns, S. E. Damborenea, M. O. Manceñido, D. J. Condon, G. N. Angelozzi, S. L. Kamo, M. Storm, A. C. Riccardi, S. P. Hesselbo, New age constraints on the Lower Jurassic Pliensbachian–Toarcian Boundary at Chacay Melehue (Neuquén Basin, Argentina). *Sci. Rep.* **12**, 4975 (2022).
51. T. H. Heimdal, Y. Goddéris, M. T. Jones, H. H. Svensen, Assessing the importance of thermogenic degassing from the Karoo Large Igneous Province (LIP) in driving Toarcian carbon cycle perturbations. *Nat. Comm.* **12**, 6221 (2021).
52. R. A. Duncan, P. R. Hooper, J. Rehacek, J. S. Marsh, A. R. Duncan, The timing and duration of the Karoo igneous event, southern Gondwana. *J. Geophys. Res.* **102**, 18127–18138 (1997).
53. T. R. Riley, I. Millar, M. K. Watkeys, M. L. Curtis, P. T. Leat, M. B. Klausen, C. M. Fanning, U–Pb zircon (SHRIMP) ages for the Lebombo rhyolites, South Africa: Refining the duration of Karoo volcanism. *J. Geol. Soc. London* **161**, 547–550 (2004).
54. F. Jourdan, G. Féraud, H. Bertrand, A. B. Kampunzu, G. Tshoso, M. K. Watkeys, B. le Gall, Karoo large igneous province: Brevity, origin, and relation to mass extinction questioned by new $^{40}Ar/^{39}Ar$ age data. *Geology* **33**, 745–748 (2005).
55. H. Svensen, S. Planke, L. Chevallier, A. Malthe-Sørenssen, F. Corfu, B. Jamtveit, Hydrothermal venting of greenhouse gases triggering Early Jurassic global warming. *Earth Planet. Sci. Lett.* **256**, 554–566 (2007).
56. H. Svensen, F. Corfu, S. Polteau, Ø. Hammer, S. Planke, Rapid magma emplacement in the Karoo Large Igneous Province. *Earth Planet. Sci. Lett.* **325–326**, 1–9 (2012).
57. A. V. Ivanov, S. Meffre, J. Thompson, F. Corfu, V. S. Kamenetsky, M. B. Kamenetsky, E. I. Demonterova, Timing and genesis of the Karoo-Ferrar large igneous province: New high precision U-Pb data for Tasmania confirm short duration of the major magmatic pulse. *Chem. Geol.* **455**, 32–43 (2017).
58. M. Moulin, F. Fluteau, V. Courtillot, J. Marsh, G. Delpech, X. Quidelleur, M. Gérard, Eruptive history of the Karoo lava flows and their impact on early Jurassic environmental change. *J. Geophys. Res. Solid Earth* **122**, 738–772 (2017).
59. N. D. Greber, J. H. F. L. Davies, S. P. Gaynor, F. Jourdan, H. Bertrand, U. Schaltegger, New high precision U-Pb ages and Hf isotope data from the Karoo large igneous province; implications for pulsed magmatism and early Toarcian environmental perturbations. *Res. Geochem.* **1**, 100005 (2020).
60. F. Jourdan, H. Bertrand, U. Schärer, J. Blichert-Toft, G. Féraud, A. B. Kampunzu, Major and trace element and Sr, Nd, Hf, and Pb isotope compositions of the Karoo Large Igneous Province, Botswana–Zimbabwe: Lithosphere vs mantle plume contribution. *J. Petrol.* **48**, 1043–1077 (2007).
61. T. H. Torsvik, M. A. Smethurst, K. Burke, B. Steinberger, Large igneous provinces generated from the margins of the large low-velocity provinces in the deep mantle. *Geophys. J. Int.* **167**, 1447–1460 (2006).
62. K. Burke, B. Steinberger, T. H. Torsvik, M. A. Smethurst, Plume generation zones at the margins of large low shear velocity provinces on the core-mantle boundary. *Earth Planet. Sci. Lett.* **265**, 49–60 (2008).
63. T. H. Torsvik, K. Burke, B. Steinberger, S. J. Webb, L. D. Ashwal, Diamonds sampled by plumes from the core-mantle boundary. *Nature* **466**, 352–355 (2010).
64. T. H. Torsvik, R. van der Voo, P. V. Doubrovine, K. Burke, B. Steinberger, L. D. Ashwal, R. G. Trønnes, S. J. Webb, A. L. Bull, Deep mantle structure as a reference frame for movements in and on the Earth. *Proc. Natl. Acad. Sci. U.S.A.* **11**, 8735–8740 (2014).
65. B. Steinberger, E. Bredow, S. Lebedev, A. Schaeffer, T. H. Torsvik, Widespread volcanism in the Greenland-North Atlantic region explained by the Iceland plume. *Nat. Geosci.* **12**, 61–68 (2019).
66. N. L. Celli, S. Lebedev, A. J. Schaeffer, C. Gaina, African cratonic lithosphere carved by mantle plumes. *Nat. Commun.* **11**, 92 (2020).
67. K. J. Matthews, K. T. Maloney, S. Zahirovic, S. E. Williams, M. Seton, R. D. Müller, Global plate boundary evolution and kinematics since the late Paleozoic. *Glob. Planet. Change* **146**, 226–250 (2016).
68. R. D. Müller, J. Cannon, X. Qin, R. J. Watson, M. Gurnis, S. Williams, T. Pfaffelmoser, M. Seton, S. H. J. Russell, S. Zahirovic, GPlates: Building a virtual Earth through deep time. *Geochem. Geophys. Geosystems.* **19**, 2243–2261 (2018).
69. T. H. Torsvik, R. van der Voo, U. Preeden, C. Mac Niocaill, B. Steinberger, P. V. Doubrovine, D. J. J. van Hinsbergen, M. Domeier, C. Gaina, E. Tohver, J. G. Meert, P. J. A. McCausland, L. R. M. Cocks, Phanerozoic polar wander, palaeogeography and dynamics. *Earth Sci. Rev.* **114**, 325–368 (2012).
70. T. H. Torsvik, B. Steinberger, L. R. M. Cocks, K. Burke, Longitude: Linking Earth's ancient surface to its deep interior. *Earth Planet. Sci. Lett.* **276**, 273–282 (2008).
71. S. Zahirovic, R. D. Müller, M. Seton, N. Flament, Tectonic speed limits from plate kinematic reconstructions. *Earth Planet. Sci. Lett.* **418**, 40–52 (2015).
72. G. E. Shephard, H.-P. Bunge, B. S. A. Schuberth, R. D. Müller, A. S. Talsma, C. Moder, T. C. W. Landgrebe, Testing absolute plate reference frames and the implications

for the generation of geodynamic mantle heterogeneity structure. *Earth Planet. Sci. Lett.* **317**, 204–217 (2012).
73. D. G. van der Meer, W. Spakman, D. J. J. van Hinsbergen, M. L. Amaru, T. H. Torsvik, Towards absolute plate motions constrained by lower-mantle slab remnants. *Nat. Geosc.* **3**, 36–40 (2010).
74. D. J. J. van Hinsbergen, L. V. de Groot, S. J. van Schaik, W. Spakman, P. K. Bijl, A. Sluijs, C. G. Langereis, H. Brinkhuis, A Paleolatitude calculator for Paleoclimate studies (model version 2.1). *PLOS ONE* **10**, e0126946 (2015).
75. K. R. Anderson, M. P. Polland, Abundant carbon in the mantle beneath Hawai'i. *Nat. Geosc.* **10**, 704–708 (2017).
76. A. Aiuppa, F. Casetta, M. Coltorti, V. Stagno, G. Tamburello, Carbon concentration increases with depth of melting in Earth's upper mantle. *Nat. Geosc.* **14**, 697–703 (2021).
77. P. H. Barry, Enriched carbon source detected. *Nat. Geosc.* **10**, 625–627 (2017).
78. H. H. Svensen, Ø. Hammer, L. Chevallier, D. A. Jerram, P. Silkoset, S. Polteau, S. Planke, Understanding thermogenic degassing in large igneous provinces: Inferences from the geological and statistical characteristics of breccia pipes in the western parts of the Karoo Basin, in T. Adatte, D. P. G. Bond, G. Keller, eds., Mass Extinctions, Volcanism, and Impacts: New Developments: Geological Society of America Special Paper 544 (2020).
79. G. R. Dickens, M. M. Castillo, J. C. G. Walker, A blast of gas in the latest Paleocene: Simulating first-order effects of massive dissociation of oceanic methane hydrate. *Geology* **25**, 259–262 (1997).
80. M. Ruhl, N. R. Bonis, G. J. Reichart, J. S. S. Damsté, W. M. Kürschner, Atmospheric carbon injection linked to end-Triassic mass extinction. *Science* **333**, 430–434 (2011).
81. W. Ruebsam, B. Mayer, L. Schwark, Cryosphere carbon dynamics control early Toarcian global warming and sea level evolution. *Glob. Planet. Change* **172**, 440–453 (2019).
82. R. Bonadio, W. H. Geissler, S. Lebedev, J. Fullea, M. Ravenna, N. L. Celli, W. Jokat, M. Jegen, C. Sens-Schönfelder, K. Baba, Hot upper mantle beneath the Tristan Da Cunha hotspot from probabilistic rayleigh-wave inversion and petrological modeling. *Geochem. Geophys. Geosystems* **19**, 1412–1428 (2018).
83. M. K. Reichow, M. S. Pringle, A. I. al'Mukhamedov, M. B. Allen, V. L. Andreichev, M. M. Buslov, C. E. Davies, G. S. Fedoseev, J. G. Fitton, S. Inger, A. Y. Medvedev, C. Mitchell, V. N. Puchkov, I. Y. Safonova, R. A. Scott, A. D. Saunders, The timing and extent of the eruption of the Siberian Traps large igneous province: Implications for the end-Permian environmental crisis. *Earth Planet. Sci. Lett.* **277**, 9–20 (2009).
84. L. E. Augland, V. V. Ryabov, V. A. Vernikovsky, S. Planke, A. G. Polozov, S. Callegaro, D. A. Jerram, H. H. Svensen, The main pulse of the Siberian Traps expanded in size and composition. *Sci. Rep.* **9**, 18723 (2019).
85. A. L. Peace, J. J. J. Phethean, D. Franke, G. R. Foulger, C. Schiffer, J. K. Welford, G. McHone, S. Rocchi, M. Schnabel, A. G. Doré, A review of pangaea dispersal and large igneous provinces—In search of a causative mechanism. *Earth Sci. Rev.* **196**, 102865 (2019).
86. S. Kender, K. Bogus, G. K. Pedersen, K. Dybkjær, T. A. Mather, E. Mariani, A. Ridgwell, J. B. Riding, T. Wagner, S. P. Hesselbo, M. J. Leng, Paleocene/Eocene carbon feedbacks triggered by volcanic activity. *Nat. Comms.* **12**, 5186 (2021).
87. S. A. Halldórsson, D. R. Hilton, P. Scarsi, T. Abebe, J. Hopp, common mantle plume source beneath the entire East African Rift System revealed by coupled helium-neon systematics. *Geophys. Res. Lett.* **41**, 2304–2311 (2014).
88. S. E. Hansen, A. A. Nyblade, M. H. Benoit, Mantle structure beneath Africa and Arabia from adaptively parameterized P-wave tomography: Implications for the origin of Cenozoic Afro-Arabian tectonism. *Earth Planet. Sci. Lett.* **319-320**, 23–34 (2012).
89. C. Civiero, J. O. S. Hammond, S. Goes, S. Fishwick, A. Ahmed, A. Ayele, C. Doubre, B. Goitom, D. Keir, J. M. Kendall, S. Leroy, G. Ogubazghi, G. Rümpker, G. W. Stuart, Multiple mantle upwellings in the transition zone beneath the northern East-African Rift system from relative P-wave travel-time tomography. *Geochem. Geophys. Geosyst.* **16**, 2949–2968 (2015).
90. E. L. Emry, Y. Shen, A. A. Nyblade, A. Flinders, X. Bao, Upper mantle Earth structure in africa from full-wave ambient noise tomography. *Geochem. Geophys. Geosystems.* **20**, 120–147 (2019).
91. A. Koptev, E. Burov, T. Gerya, L. le Pourhiet, S. Leroy, E. Calais, L. Jolivet, Plume-induced continental rifting and break-up in ultra-slow extension context: Insights from 3D numerical modeling. *Tectonophysics* **746**, 121–137 (2018).
92. A. A. Nyblade, R. A. Brazier, Precambrian lithospheric controls on the development of the East African rift system. *Geology* **30**, 755–758 (2002).
93. G. E. M. Hall, P. Pelchat, Evaluation of a direct solid sampling atomic absorption spectrometer for the trace determination of mercury in geological samples. *Analyst* **122**, 921–924 (1997).
94. C. Bin, W. Xiaoru, F. S. C. Lee, Pyrolysis coupled with atomic absorption spectrometry for the determination of mercury in Chinese medicinal materials. *Anal. Chim. Acta* **447**, 161–169 (2001).
95. S. P. Hesselbo, C. J. Bjerrum, L. A. Hinnov, C. MacNiocaill, K. G. Miller, J. B. Riding, B. van de Schootbrugge, The Mochras Revisited Science Team, Mochras borehole revisited: A new global standard for Early Jurassic Earth history. *Sci. Drill.* **16**, 81–91 (2013).
96. D. R. Tappin, R. A. Chadwick, A. A. Jackson, R. T. R. Wingfield, N. J. P. Smith, Geology of Cardigan Bay and the Bristol Channel, United Kingdom Offshore Regional Report. British Geological Survey, HMSO. (1994) pp. 107.
97. P. Copestake, B. Johnson, Lower Jurassic Foraminifera from the Llanbedr (Mochras Farm) Borehole, North Wales, UK. *Monogr. Palaeontographical Soc.* **167**, 403 (2014).
98. B. W. Sellwood, H. C. Jenkyns, Basins and swells and the evolution of an epeiric sea. *J. Geol. Soc. Lond.* **131**, 373–388 (1975).
99. M. Ruhl, S. P. Hesselbo, L. Hinnov, H. C. Jenkyns, W. Xu, J. B. Riding, M. Storm, D. Minisini, C. V. Ullmann, M. J. Leng, Astronomical constraints on the duration of the Early Jurassic Pliensbachian stage and global climatic fluctuations. *Earth Planet. Sci. Lett.* **455**, 149–165 (2016).
100. C. V. Ullmann, D. Szücs, M. Jiang, A. J. L. Hudson, S. P. Hesselbo, Geochemistry of macrofossil, bulk rock, and secondary calcite in the Early Jurassic strata of the Llanbedr (Mochras Farm) drill core, Cardigan Bay Basin, Wales, UK. *J. Geol. Soc. London* **179**, jgs2021-018 (2021).
101. A. Mazzini, H. Svensen, H. A. Leanza, F. Corfu, S. Planke, Early Jurassic shale chemostratigraphy and U–Pb ages from the Neuquén Basin (Argentina): Implications for the Toarcian Oceanic Anoxic event. *Earth Planet. Sci. Lett.* **297**, 633–645 (2010).
102. F. Corfu, H. Svensen, A. Mazzini, Comment to paper: Evaluating the temporal link between the Karoo LIP and climatic–biologic events of the Toarcian Stage with high precision U–Pb geochronology by Bryan Sell, Maria Ovtcharova, Jean Guex, Annachiara Bartolini, Fred Jourdan, Jorge E. Spangenberg, Jean-Claude Vicente, Urs Schaltegger in Earth and Planetary Science Letters 408 (2014) 48–56. *Earth Planet. Sci. Lett.* **434**, 349–352 (2016).
103. B. van de Schootbrugge, T. R. Bailey, Y. Rosenthal, M. E. Katz, J. D. Wright, K. G. Miller, S. Feist-Burkhardt, P. G. Falkowski, Early Jurassic climate change and the radiation of organic-walled phytoplankton in the Tethys Ocean. *Paleobiology* **31**, 73–97 (2005).
104. F. Ibanez, Effet des transformations des données dans l'analyse factorielle en écologie planctonique. *Cahiers océanographiques* **23**, 545–561 (1971).
105. P. Legendre, L. Legendre, Ordination in reduced space. *Dev. Environ. Model.* **24**, 425–520 (2012).
106. O. Hammer, D. A. T. Harper, Paleontological data analysis. Blackwell Publishing Ltd. (2007). 10.1002/9780470750711.
107. O. M. Bialik, E. Jarochowska, M. Grossowicz, Ordination analysis in sedimentology, geochemistry and palaeoenvironment—Background, current trends and recommendations. *Depositional Record* **7**, 541–563 (2021).

Acknowledgments
Funding: We acknowledge support from the National Natural Science Foundation of China (grant no. 41888101 to M.R. and W.X.), Shell International Exploration and Production B.V. (M.R., S.P.H., H.C.J., and W.X.), the UK Natural Environment Research Council (grant NE/N018508/1 to S.P.H., C.M.N., and J.B.R.), the SFI Research Centre in Applied Geosciences (iCRAG; M.R., R.L.S., and W.X.), the ERC consolidator grant ERC-2018-COG-818717-V-ECHO (T.A.M.), and the International Continental Scientific Drilling Programme (ICDP). We acknowledge support from the British Geological Survey, especially S. Renshaw and T. Gallagher, for enabling access to the Mochras core. J.B.R. publishes with the approval of the Executive Director, British Geological Survey (NERC). This manuscript is a contribution to the ICDP Integrated Understanding of the Early Jurassic Earth System and Timescale (JET) project, IGCP 632 [International Union of Geological Sciences and United Nations Educational, Scientific and Cultural Organization (IUGS-UNESCO)]: "Continental Crises of the Jurassic: Major Extinction events and Environmental Changes within Lacustrine Ecosystems," IGCP 655 (IUGS-UNESCO): "Toarcian Oceanic Anoxic Event: Impact on marine carbon cycle and ecosystems," and IGCP 739 (IUGS-UNESCO): "The Mesozoic–Palaeogene Hyperthermal events."
Author contributions: Conceptualization: M.R. and S.P.H. Methodology: M.R., R.L.S., and T.A.M. Investigation: M.R., S.P.H., H.C.J., W.X., K.J.M., R.L.S., and J.B.R. Visualization: M.R. and R.L.S. Writing (original draft): M.R., S.P.H., and R.L.S. Writing (review and editing): M.R., S.P.H., H.C.J., W.X., R.L.S., K.J.M., T.A.M., C.M.N., and J.B.R. **Competing interests:** The authors declare that they have no competing interests. **Data and materials availability:** All data needed to evaluate the conclusions in the paper are present in the paper and/or the Supplementary Materials.

Submitted 12 January 2022
Accepted 12 July 2022
Published 9 September 2022
10.1126/sciadv.abo0866

ScienceAdvances

Reduced plate motion controlled timing of Early Jurassic Karoo-Ferrar large igneous province volcanism

Micha RuhlStephen P. HesselboHugh C. JenkynsWeimu XuRicardo L. SilvaKara J. MatthewsTamsin A. MatherConall Mac NiocaillJames B. Riding

Sci. Adv., 8 (36), eabo0866. • DOI: 10.1126/sciadv.abo0866

Science Advances (ISSN) is published by the American Association for the Advancement of Science. 1200 New York Avenue NW, Washington, DC 20005. The title *Science Advances* is a registered trademark of AAAS.